Synthesis of TiO$_2$/polyaniline photocatalytic nanocomposite and its effects on degradation of metronidazole in aqueous solutions under UV and visible light radiation

Esrafil Asgari[a], Ali Esrafili[b,c], Ahmad Jonidi Jafari[b,c], Roshanak Rezaei Kalantary[b,c], Mahdi Farzadkia[b,c],*

[a]*Department of Environmental Health Engineering, Khoy University of Medical Sciences, Khoy, Iran, email: sasgary@gmail.com*
[b]*Research Center for Environmental Health Technology, Iran university of Medical Sciences, Tehran, Iran,*
Tel. +982186704820/+98 21 88607939; Fax: +982188622707; emails: farzadkia.m@iums.ac.ir (M. Farzadkia),
a_esrafily@yahoo.com (A. Esrafili), ahmad_jonidi@yahoo.com (A.J. Jafari), rezaei.r@iums.ac.ir (R.R. Kalantary)
[c]*Department of Environmental Health Engineering, School of Public Health, Iran University of Medical Sciences, Tehran, Iran*

ABSTRACT

TiO$_2$/polyaniline (TiO$_2$/Pani) nanocomposite was prepared by in situ polymerization of aniline on TiO$_2$ nanoparticle structures. Fourier transform infrared, field emission scanning electron microscopy, energy-dispersive X-ray spectroscopy, diffuse reflectance spectroscopy, and thermogravimetric analysis techniques were utilized to characterize the composition and structure of the nanocomposite and its components. All these techniques showed that TiO$_2$/Pani nanocomposite was formed successfully and thus can activate by exposure to UV and visible light. The photocatalytic activity of the synthetic nanocomposite on degradation of metronidazole (MNZ) molecules in aqueous solution was investigated under UV and visible light radiation as a function of time, MNZ concentration, catalyst dose and stability, and solution pH during several steps of the degradation process. The optimal condition for maximum MNZ degradation efficiency was obtained to be 98% and 96%, respectively, with 1 g L^{-1} of TiO$_2$/Pani nanocomposite, 10 mg L^{-1} of MNZ, and pH 7.0 after 120 min of exposure to UV and visible light. Kinetic studies, chemical oxygen demand, total organic carbon, average oxidation state, reusability test, and predicted degradation mechanism of the optimal condition were investigated in the present study. The photocatalytic activity of TiO$_2$/Pani nanocomposite under UV and visible light radiation was higher than TiO$_2$ nanoparticles. The velocity constants for MNZ degradation by TiO$_2$/Pani nanocomposite under UV and visible light radiations were 387 × 10^{-4} and 286 × 10^{-4} min^{-1}, respectively, which were approximately 1.63 and almost 95 fold over TiO$_2$. It was also confirmed that hydroxyl ($^{\bullet}$OH) and superoxide anion ($^{\bullet}$O$_2^-$) radicals, respectively, played central roles in MNZ degradation. Finally, the mechanism of increase in the photocatalytic activity was discussed. The improvement of photocatalytic activity under UV and visible light radiation was related to the remarkable absorption of UV and visible light and the reduction of recombination of the charge carriers.

Keywords: TiO$_2$ nanoparticles; Polyaniline; Photocatalytic degradation; Antibiotic; Metronidazole; UV and visible light radiation

1. Introduction

The widespread consumption of pharmaceutical and personal care products in therapeutic approaches has resulted in environmental contamination worldwide [1,2]. Among various pharmaceutical products, consumption of antibiotics is increasing rapidly and therefore many investigations have been performed concerning the presence of antibiotics in environment [1,3]. Although the antibiotic

---

* Corresponding author.

concentrations found in the environments were very limited, from ng L^{-1} to µg L^{-1} in water and µg L^{-1} to mg L^{-1} in soil, their significance is due to the development of bacterial resistance and therefore are a threat to the health of mankind [4]. Metronidazole (MNZ) ($C_6H_9N_3O_3$), which contains methyl and nitro groups, is one of the most common antibiotics belonging to the nitroimidazole class which is frequently used for treatment of various anaerobic infections such as intra-abdominal, anti-protozoal, and anti-amebae infections (Fig. 1) [4]. There is a risk for the presence of MNZ in raw waters due to the lack of molecular biodegradation and high water solubility and thus complete removal from drinking waters and wastewater have been extensively investigated by several researchers [5,6].

Biological methods are common techniques for degradation of these contaminants but cannot efficiently remove them [7]. Physical sedimentation methods such as centrifugation, coagulation, and flocculation can result in secondary contaminations [7]. Advanced oxidation processes (AOPs) have been recently used for removal of organic compounds, especially the resistant ones [8]. Among different AOPs, photocatalysis using TiO_2 (Sigma-Aldrich, US Research Nanomaterials, Inc.), which is a commercial catalyst, have been greatly considered due to high efficiency, chemical and physical stability, nontoxicity, relative cheapness and biocompatibility for water purification [9]. Exposure of TiO_2 particles to radiation of photons with higher energy levels than their energy gap (approximately 3.1 eV) can lead to production of electron–hole pair (e^-/h^+) [10], where the subsequent reaction of h^+ with H_2O or OH^- causes the creation of reactive radicals that act as strong oxidants for the absorbed contaminants. Due to the higher energy gap of TiO_2, UV radiation ($\lambda < 387$) is essential as a light resource [11]. In spite of several studies that have investigated TiO_2 photocatalyst for optical degradation of organic contaminants [12], there are still several limitations such as separation of semiconductor powders from discontinuous slurry photoreactors and high tendency for recombination of the optically produced e^-/h^+ in comparison with contribution in reactive radicals

formation that results in low photocatalytic degradation efficiency [12]. Furthermore, the UV spectrum present in sunlight is very low (<5%) and hence the use of TiO_2 photocatalysis under UV and visible light radiation is restricted [13]. Considering the limitations and harmful effects of UV radiation on human life, there is a great challenge in alteration of the activating region of ZnO or TiO_2 to visible light spectrum. This can be carried out by surface alteration and modification of TiO_2 nanoparticles by doping of metal ions [14], nonmetallic doping [14], deposition of noble metals [15], coupling with semiconductors with narrow band [16], color sensitization [17], and several other sensitization materials [18,19]. Recently, using nanocomposites based on the conductor polymers and semiconductor metallic oxides has been vastly considered and is an interesting research field due to possessing both organic and mineral properties [20]. It is reported that conductor polymers act as sensitizers for increasing the spectral response of ZnO and TiO_2 to visible light radiation [21,22]. In this respect, sensitizers are able to increase the transmission of optically produced electrons [23]. Conductor polymers (such as polyaniline, polypyrrole, and polythiophene) have been studied extensively due to their unique electrical and optical properties, such as high absorption coefficient, decent electron transmission, high electron motility, and excellent stability [24]. As a frequently used polymer, polyaniline has many advantages such as low price, high polymerization efficiency, ease of synthesis, and environmental and chemical stability [25]. The electrical, electrochemical, and optical properties of polyaniline have made it an attractive material for utilizing in the production of anti-corrosion coatings, batteries, supercapacitors, photovoltaic devices, photocatalysts, etc. For instance, production of polyaniline nanocomposites with metallic oxides such as zinc oxide [26,27], aluminum oxide [14], manganese oxide [28], iron oxide [29,30], titanium oxide [9,30], as well as nanostructures such as carbon nanotube [31], graphite [32,33], and montmorillonite [34] is reported. The use of polyaniline to improve the photocatalytic activity of TiO_2 nanoparticles has been extensively studied [24]. With an extended π conjugate system, polyaniline enhances the optically produced charges and prevents e^-–h^+ recombination [24]. During TiO_2/Pani photocatalysis, Pani absorbs the light so that excited electrons can migrate to the conduction band [35] of TiO_2 and the holes formed in the TiO_2 valence band (VB) can be directly transferred to HOMO Pani orbital. Therefore, the recombination of electron–hole pair is strongly inhibited and optical response and electrical properties of TiO_2/Pani nanocomposite are improved [36,37]. Afterwards, the electrons are transferred to the nanocomposite surface where they can react with water and oxygen to form hydroxyl and superoxide radicals that can oxidize or degrade organic molecules [28].

In a study regarding synthesis of polypyrrole/titanium dioxide nanocomposite and its activity on degradation of methyl orange and methylene blue under visible light radiation, it was observed that by increasing polypyrrole amounts, the photocatalytic activity was also increased [38,39]. Guo et al. [40] produced TiO_2/Pani composite by sol-gel method and found that there was a synergic effect between Pani and TiO_2 nanocomposites under both UV and sunlight radiation which led to the reduction of electron–hole
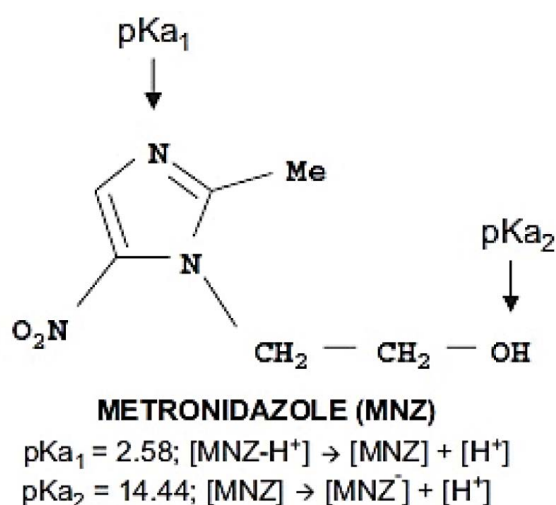

Fig. 1. Chemical structure and acidity constants of metronidazole powder.

recombination as well as the increased photocatalytic activity that led to the degradation of Congo Red (CR) and Methyl Orange (MO). Gu et al. [41] reported photocatalytic degradation of rhodamine B using TiO_2/Pani composite and their results revealed that the synthetic composite acted as a very efficient photocatalyst when exposed to visible light radiation. In this respect, other research groups observed a similar trend for the increase of photocatalysis using TiO_2 modified with Pani comparing with pure TiO_2 [42]. Li et al. [36] prepared modified TiO_2 with Pani by in situ chemical oxidative polymerization in which the increase of photocatalytic activity on degradation of ethylene di amine tetra acetic acid under visible light radiation was 4.6 times higher due to the synergic effects between Pani and TiO_2. In another study, composite films of TiO_2/Pani were prepared by electrochemical anodic oxidation and results showed that the optical flow was increased approximately 2.5 folds comparing with pure TiO_2 [43]. To the best of our knowledge, degradation of metronidazole using sensitized TiO_2 with polyaniline under UV and visible light radiation has not yet been assessed. In the present study, we synthesized TiO_2/Pani nanocomposites by in situ polymerization of aniline together with TiO_2 nanoparticles and investigated its photocatalytic activity on degradation of a pharmaceutical contaminant (MNZ) in water under UV and visible light radiation. The synthetic TiO_2/Pani nanocomposite was characterized by Fourier transform infrared (FTIR), field emission scanning electron microscopy (FESEM), energy-dispersive X-ray spectroscopy (EDX), UV–Vis diffuse reflectance spectroscopy (DRS), and thermogravimetric analysis (TGA) techniques. Moreover, the operational conditions for photocatalytic removal of MNZ were optimized by TiO_2/Pani nanocomposite. Based on the results, the removal of MNZ was performed under the optimal conditions by means of a very low TiO_2/Pani dose and less contact time.

2. Materials and methods

2.1. Chemicals and instruments

Aniline (99.5%, Sigma-Aldrich, USA), TiO_2 Degussa P25 (nanopowder size < 30 nm particle, Sigma-Aldrich), sulfuric acid (H_2SO_4) (Merck, Germany), ether (Merck, Germany), ethanol (Merck, Germany), and ammonium persulfate $(NH_4)_2S_2O_8$ (APS, Merck, Germany) were mainly used without purification. Metronidazole (99%, chemical reagent) was purchased from Merck co. (Darmstadt, Germany) and used without purification. High-performance liquid chromatography (HPLC) (Cecil 4100 Powerstream Interface, UK) was used for determination of remaining MNZ. The pH of the solutions was measured with Metrohm pH meter (model-827, Switzerland). COD was determined with COD reactor model AR851 (HACH, USA) using standard method [44]. The efficiency of TiO_2/Pani nanocomposite in mineralization of MNZ molecules was assessed with a total organic carbon analyzer (Multi N/C 3100, TOC analyzer, Germany). Distilled water was used for preparation of all solutions. All reactors involved in the experiments possessed an analytical grade. The average oxidation state (AOS) was calculated according to Eq. (1):

$$AOS = 4 - 1.5 \frac{COD}{TOC} \qquad (1)$$

In which, the range of AOS is between –4 and +4 for methane and carbon dioxide, respectively [45].

2.2. Synthesis of Pani and TiO_2/Pani nanocomposite

TiO_2/Pani nanocomposite was prepared by chemical in situ polymerization of aniline (An) using ammonium persulfate (APS) as an oxidant in the presence of TiO_2. The molar ratio of An:APS was maintained at 1:1.25 and its effect on the synthesis was assessed [46]. TiO_2/Pani samples were prepared with predefined weight percentages [(5%) m(An)/m(TiO_2)]. The preferred mass for TiO_2 was estimated to be 4 g. TiO_2/Pani nanocomposite was prepared using the solutions below: the water solution A (50 mL) containing 4 g TiO_2 and 0.055 mL H_2SO_4 which was exposed to ultrasound for 15 min to form a stable suspension, the water solution B (50 mL) containing 0.196 mL aniline and 0.055 mL H_2SO_4, and the water solution C (50 mL) which contained 0.613 g APS and 0.055 H_2SO_4.

200 mL of aqueous solutions A and B were added to the reactor and the suspension was mixed for 15 min (650 rpm) to more stability of TiO_2. In situ polymerization was initiated by addition of one drop of solution C to the reactor and the volume was reached to 200 mL by adding water. The polymerization solution was mixed for 24 h at room temperature and the dark green product was separated by centrifugation. The produced nanocomposites were washed vigorously in deionized water. For removal of oligomers, the powder was extracted with ethanol and then washed with 50 mL of ethanol and 30 mL of ether. The sediment was dried for 24 h at 60°C. The pure form of Pani was prepared as described before, without addition of TiO_2 nanoparticles [47]. Weight percentages of 1 and 10 for aniline used in the nanocomposite were also prepared as described above.

2.3. TiO_2/Pani nanocomposite characteristics and its components

FTIR spectra for TiO_2/Pani nanocomposite and its components were recorded using KBr tablets on a Perkin-Elmer Frontier spectrometer (PerkinElmer Corp., USA). The spectra were collected in 20 scans from 4,000 to 400 cm^{-1} with a resolution of 4 cm^{-1}. Surface morphology of the nanocomposite was observed with SEM analysis. Chemical composition of the catalysts was determined by EDX along with SEM. Images of FESEM for TiO_2/Pani nanocomposite and its components were recorded with MIRA3-XMU microscopy (TESCAN Corp., Czech Republic). The wavelengths for optical activation of TiO_2/Pani nanocomposite and its components were assessed by ultraviolet-visible DRS (PerkinElmer Corp., USA). TGA [48] for measurement of thermal degradation of TiO_2/Pani nanocomposite powders was achieved using STA504 system with a scanning rate from 10°C min^{-1} to 600°C.

Remaining concentration of MNZ was measured with HPLC device containing a diode array detector UV–Visible (4900 CE) which was set for 317 nm. A C18 column (5 μm, 250 mm × 4.6 mm) was utilized. The data were assessed with ChemiStation software. The moving phase consisted of a mixture of acetonitrile and distilled water (volume ratio 30:70). The flow rate was approximately 1 mL min^{-1} and the injection volume was 20 μL [49]. The maintenance time for

MNZ was 5 min. The sample of regular HPLC for MNZ is presented in Fig. 2. The antibiotic solution was prepared by solving 10 mg MNZ in 1 L of distilled water. The initial COD of MNZ aqueous solution with concentration of 10 mg L^{-1}, equals to 126 mg L^{-1}. The antibiotic solution was prepared weekly and kept at 4°C.

2.4. Photocatalytic system

Schematic diagram of the reactor used for MNZ photocatalysis is shown in Fig. 3. The reactor was consisted of three parts: (A) the internal part containing a central UV or xenon lamp, (B) the external part containing a 2 L solution, and (C) a thermometer to maintain the reactor solution temperature in an approximate range of 24°C ± 2°C by cold-water pipes rotating around the reactor. Total volume of the reactor was 2 L with a working volume of 1 L. The reactor solution was mixed constantly through a magnetic stirrer (170 rpm). The photocatalytic activity was assessed by MNZ degradation under visible light ($\lambda > 400$ nm) and UVA light ($\lambda = 365$ nm) radiation. The visible light was obtained by a 300 W xenon lamp (Osram XBO, Germany) with a 400 nm filter to ensure the transmission of the desired light. Average light intensity of the xenon lamp was
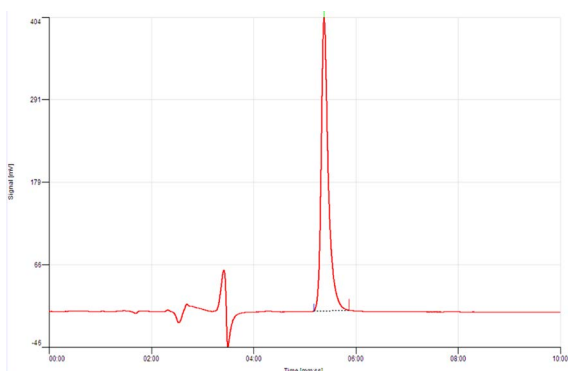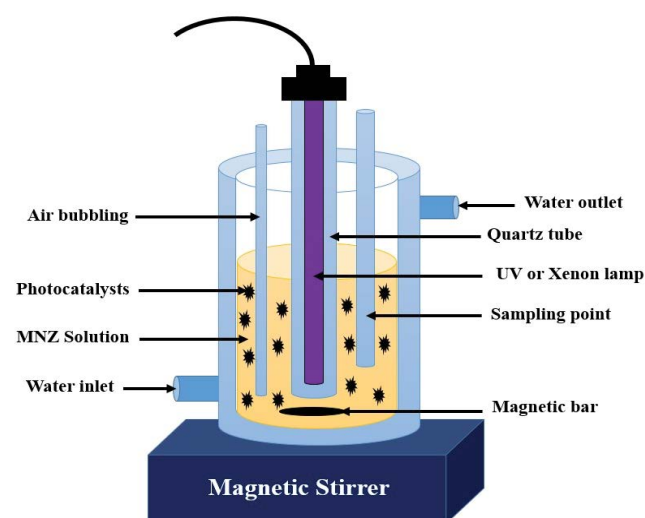

Fig. 2. A regular HPLC chromatogram of MNZ.

Fig. 3. Schematic diagram of the reactor used.

2,650 μm cm^{-2}. The UVA light was obtained by a 36 W UVA light bulb (Philips, Netherlands, 46 cm in length, 2.5 cm in diameter) with a moderate intensity of 3,100 μm cm^{-2}. The light intensity was measured with a digital radiometer/photometer (XP-2000, Accu PRO™, UK).

2.5. Removal experiments

In discontinuous experiments, an amount of 0.5–1.0 g L^{-1} selected from TiO$_2$/Pani nanocomposite was added to 1,000 mL of MNZ solution with predefined concentration (10–40 mg L^{-1}) in different pH, ranging from 3.0 to 10. The stock solution (1,000 mg L^{-1}) was prepared with pure MNZ powder. The initial pH was adjusted by addition of NaOH and HCl (0.1 N) and measured with a pH meter. All experiments were carried out for 3 h under environmental conditions. Before each experiment, the reactor was put in the dark and the MNZ solution was stirred for 30 min to reach the adsorption equilibrium. After the equilibrium period, the lamp was turned on and 10 mL of the solution was taken at certain time intervals. The water samples were spun for 10 min at 4,000 rpm with a centrifugation device (Sigma-301, Germany) to remove TiO$_2$/Pani nanocomposite and afterwards the remaining MNZ concentration was measured. The removal efficiency (%) was calculated according to Eq. (2) as follows:

$$\text{Removal efficiency}\left(\%\right) = \frac{\left(C_0 - C\right)}{C_0} \times 100 \qquad (2)$$

where C_0 and C are MNZ concentrations (mg L^{-1}) initially and at time t. To ensure accuracy of the results, all experiments were repeated three times and the average results were reported.

3. Findings and discussion

3.1. Characteristics of the nanocomposite

3.1.1. FTIR analysis

FTIR analysis was used for detection of functional groups on the nanocomposite surface. FTIR spectra for Pani, TiO$_2$, and TiO$_2$/Pani nanocomposite was recorded in the range of 4,000–400 cm^{-1} and presented in Fig. 4.

In FTIR spectrum of Pani emeraldine salt, the specific absorption bands observed in 812; 1,119; 1,297; 1,500; 1,580; and 3,174 cm^{-1} are successively attributed to C–N–C bond mode in the aromatic ring, N=Q=N bond mode (*Q* represents the quinoid unit), stretching vibrational mode in benzenoid units C–N, C=C, C=C of the quinoid units, and N–H [43]. A specified peak can be observed at 511 cm^{-1} in the TiO$_2$ spectrum which is related to stretching vibrational mode of Ti–O–Ti bonds [9]. The peaks at 1,499 and 3,173 cm^{-1} are attributed to stretching vibrational mode of the hydroxyl groups.

In the FT-IR spectrum of TiO$_2$/Pani nanocomposite, the specified absorption bands of Pani are moved to 511; 1,151; 1,309; 1,500; 1,590; and 3,143 cm^{-1}. Due to the presence of TiO$_2$ in TiO$_2$/Pani nanocomposite, the peak resulted from stretching vibrational mode of C–N of the benzenoid units existing in Pani has moved from 1,297 to 1,309 cm^{-1}, indicating
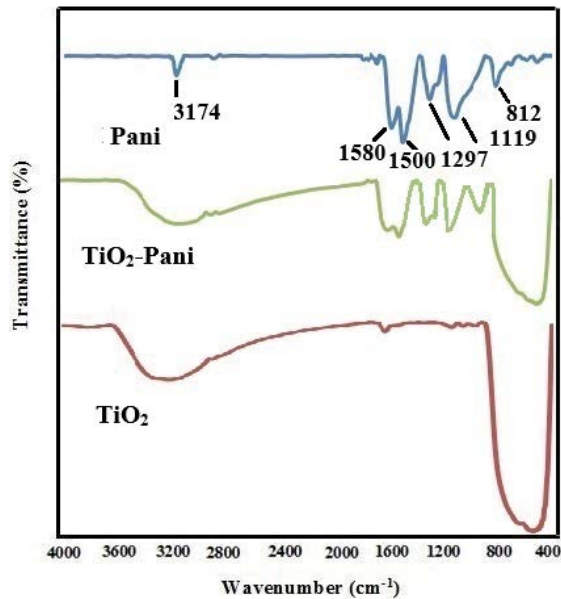
Fig. 4. FTIR spectra for Pani, TiO_2, and TiO_2/Pani nanocomposite powders.

reaction of the nitrogen atoms in C–N bond of Pani and the oxygen atoms of TiO_2 [46,50]. Moreover, all Pani bands are shifted to longer wavelengths which demonstrates electron transmission between Pani and TiO_2 nanoparticles [43]. In other words, this indicates the presence of physicochemical reactions, such as hydrogen bonds, between

TiO_2 nanoparticles and the amino groups of Pani molecules [47]. However, the visually observable color change from white to green in TiO_2 nanoparticles after purification with the Pani confirms the presence of Pani on the surface of TiO_2 nanoparticles in the emeraldine salt form [47]. Similar findings were reported by several research groups [46,47].

3.1.2. FESEM and EDX analysis

FESEM was used for surface morphological studies of Pani, TiO_2 nanoparticles, and TiO_2/Pani nanocomposite. FESEM and EDX images are shown in Fig. 5. Fig. 5a shows an even and dense FESEM image for Pani with an approximate diameter of 40–80 nm. Fig. 5b shows FESEM image of TiO_2 nanoparticles with an approximate diameter of 30 nm and their crystalline structure. In comparison with TiO_2 (Fig. 5b), TiO_2/Pani nanocomposite (Fig. 5c) had smoother interfacial intervals indicating that TiO_2 and TiO_2/Pani layers were successfully formed. The TiO_2/Pani nanocomposites were spherical shaped and evenly distributed with an approximate diameter of 35 nm. FESEM images of TiO_2 and TiO_2/Pani were not changed before and after the modification by Pani which shows that the coated Pani layer was very thin.

Comparing with TiO_2, TiO_2/Pani nanocomposite had a lower dispersion degree and accumulation because of the oxidation polymerization reaction and the absorption of Pani. Due to surface effects, these nanocomposites can improve charge transmission capacity [21,43]. Elemental analysis of the catalyst resulted from EDX of Pani, TiO_2 nanoparticles,
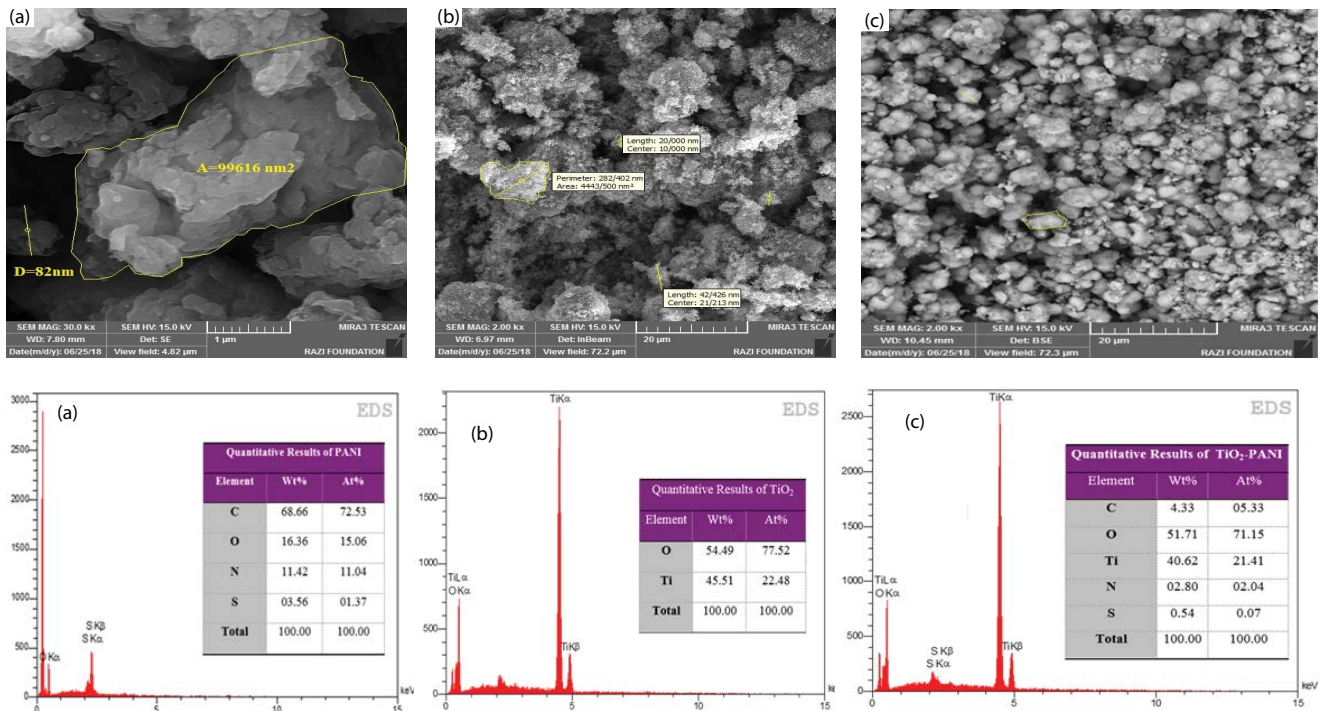

Fig. 5. Images of scanned electron microscopy and X-ray dispersing spectra of (a) Pani, (b) TiO_2, and (c) TiO_2/Pani nanocomposite powders.

and TiO$_2$/Pani nanocomposite were summarized in Fig. 5. Figs. 5a–c confirm the presence of C, O, N, Ti, and S in the TiO$_2$/Pani nanocomposite, whereas the presence of C, O, N, and S together with Ti in TiO$_2$/Pani nanocomposite is an evidence suggesting the presence of polyaniline chains in TiO$_2$ nanoparticles.

3.1.3. UV–Vis diffuse reflectance spectra and band gap studies

To assess the responses of samples to UV and visible light radiation, Pani, TiO$_2$ nanoparticles, and TiO$_2$/Pani nanocomposites were identified by UV–Vis diffuse reflection spectroscopy (Fig. 6a). The absorption spectrum of TiO$_2$ nanoparticles shows a sharp absorption peak at about 390 nm, indicating a single specified peak. Pani shows absorption of both UV and visible light which is in consistency with the other studies (Fig. 6a) [40,51]. Furthermore, Pani shows two specified absorption bands at 360 and 450 nm. The first band is a result of antibonding polaron state (type π–π*) of the benzenoid units and the second band is caused by doping amount of the quinoid units. The type of the dopant used has a great effect on the properties of the nanocomposites [42,52]. In scientific literature, Pani absorption peaks detected in range of 700–800 nm are attributed to presence of acidic solvents used for aniline polymerization [47]. It has been recently shown that the doping-undoping processes that occur upon oxidation/reduction of conducting polymers are not as simple as being described at the early stage of their discoveries [53]. It is a complex behavior of distinct anion and cation transport processes that occur at the solid-state polymeric electrode/solution interface during the redox reaction [54]. There is a need for an online/real-time technique for in-situ monitoring of what happens during the redox reactions or doping–undoping processes of conducting polymers [54]. Any interaction with Pani which affects the number and movement of charge carriers along the chain or by transfer of charge carriers between chains will affect the conductivity of doped Pani [42]. The UV–Visible spectrum of TiO$_2$/Pani nanocomposite (Fig. 6a) showed a peak at 430 nm which was altered compared with the unmodified peaks of Pani (450 nm) and

TiO$_2$ nanoparticles (390 nm). This demonstrates a strong reaction between the polymer and the nanoparticles which can simplify charge transmission from Pani to TiO$_2$ through hydrogen bonds. This leads to alteration of the absorbed wavelength. Similar results in other studies using TiO$_2$/Pani [24,43] revealed that the synthetic nanocomposites were sensitized to increase the response to visible light through specific surface structure of TiO$_2$ nanoparticles and combining with Pani. This phenomenon increases the separation of charge carriers and, as a result, improves photocatalytic activity.

Energy of the gap band of photocatalyst was obtained according to Eq. (3):

$$E_g \left(\text{eV} \right) = \frac{1,240}{\lambda} \tag{3}$$

where E_g is the energy of gap band (eV) and λ is the wavelength of absorption edge [51]. The energies of the gap band for TiO$_2$ and TiO$_2$/Pani were 3.17 and 2.88 eV, respectively. The optical gap band of TiO$_2$/Pani nanocomposite and its pure components were determined using Tauc plot via modified Kubelka-Munk [55] function with linear extrapolation (Fig. 6b) [51].

3.1.4. Thermogravimetric analysis

Thermal behavior of TiO$_2$, Pani, and TiO$_2$/Pani was assessed by TGA and the results are depicted in Fig. 7. The blue curve indicates that TiO$_2$ was very stable in the air and not degraded in thermal range of 30°C–600°C (Fig. 7a). The thermogravimetry results of Pani and TiO$_2$/Pani were successively shown as black and red curves in Figs. 7b and c, where the mass reduction of samples was observed from 25°C to 600°C. The severe mass reduction observed below 200°C might be due to evaporation of the water molecules absorbed on nanocomposite surface. The severe mass reduction which is also observed in the range of 200°C–600°C is mainly due to degradation of polyaniline chains [36,51]. Also, massive weight loss from 400°C onward is due to the thermooxidative decomposition of Pani, which may involve
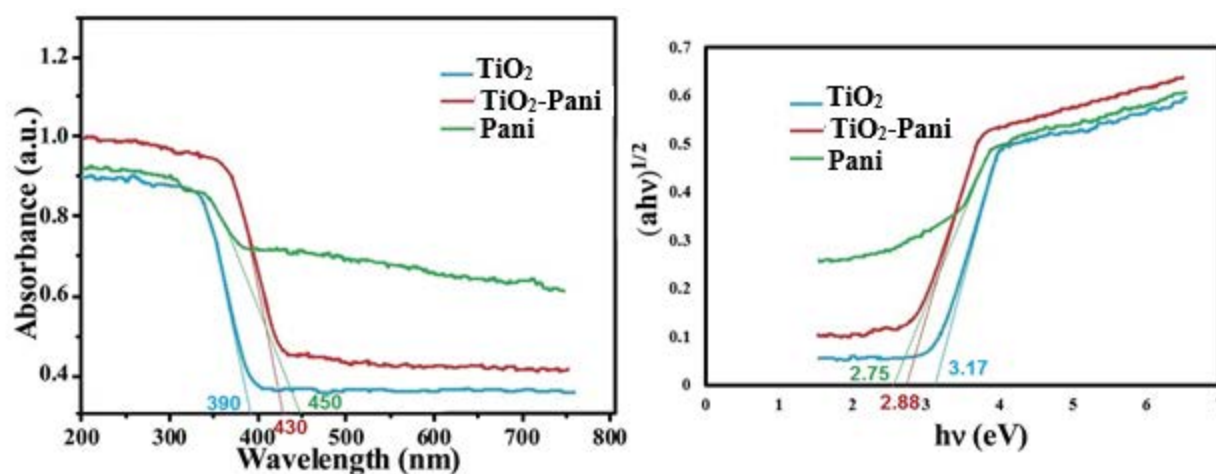

Fig. 6. Diffuse reflectance spectrometry (DRS) of UV-Visible from (a) TiO$_2$, Pani, and TiO$_2$/Pani nanocomposite, and (b) optical gap band (Tauc plot).
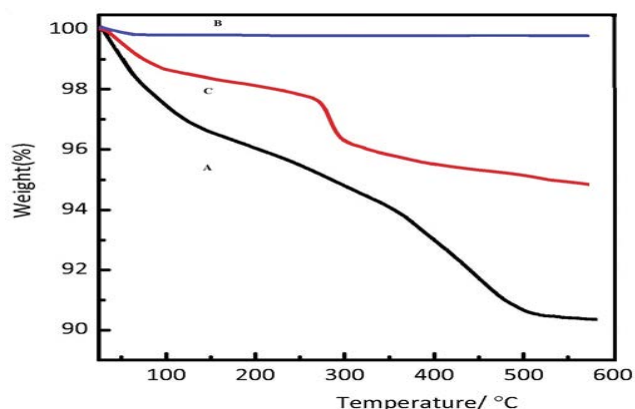
Fig. 7. Thermogravimetry analysis curves for (a) Pani, (b) TiO_2, and (c) TiO_2/Pani nanocomposite.

the evolution of degradation products such as ammonia, aniline, *p*-phenylenediamine, *N*-phenylaniline, *N*-phenyl-1,4-benzenediamine, carbazole, pyridine-based heterocycle, methane, acetylene, etc [42]. The weight percentage of Pani was estimated about 5%, respecting the weight loss.

3.2. Photocatalytic degradation of metronidazole

3.2.1. Effect of pH

The solution pH is one of the most important parameters affecting ionization properties of the contaminator and surface properties of the photocatalyst and thus can determine type of dominant radicals involved in AOP and consequently affect the process efficiency [51,56]. Various studies have revealed that pH plays an important role in degradation and removal of antibiotics [7,49]. Herein, the effect of pH in TiO_2/Pani photocatalysis was assessed for MNZ degradation efficiency at different radiation exposure times under UV and visible light. The results showed that maximum removal percentages under UV and visible light after 2 h in pH 10 were, respectively, ~100% and 97% and in pH 7.0 were 98% and 96%. Minimum removal percentages were observed in pH 3.0, which were 70.5% and 67.8% (Fig. 8a). This means that to obtain economically higher

efficiency, photocatalytic degradation of MNZ should be carried out in neutral pH.

Fig. 8a represents optimal condition for photocatalytic degradation of MNZ after 120 min exposure to UV and visible light in pH 7.0. As you see, removal efficiency is directly related to the exposure time and increase of pH. Surface modification of polar TiO_2 nanoparticles by polyaniline chains can alter their surface properties and zero point charge. Zero point charges for TiO_2 and TiO_2/Pani were 6.21 ± 0.2 and 7.64 ± 0.3, respectively (Fig. 9). In this respect, the aforementioned nanocomposite had a positive charge at $pH < pH_{zpc}$ and negative charge at $pH > pH_{zpc}$ [56]. Therefore, reduction of MNZ removal efficiency in strong acidic and basic conditions could be explained by pK_a of MNZ (2.55) and pH_{zpc} of TiO_2/Pani nanocomposite (8.1), such that electrostatic interaction is improved in higher pH values which leads to increase of surface absorption by the photocatalyst and increase of photocatalytic activity. Furthermore, absorption of MNZ by TiO_2/Pani nanocomposite in neutral condition (pH 7.0) could be due to the hydrogen bonds and the interaction of π–π^* between MNZ and TiO_2/Pani. On the other hand, amount of hydroxyl ions (OH^-) is increased in higher pH values and thus through the reaction of h^+ and OH^- free $\cdot OH$ radicals are produced. Therefore high values of pH are beneficial for photocatalysis [51].

MNZ is an electron deficient molecule and its aromatic structure act as a π electron acceptor which can be absorbed on TiO_2/Pani surface through the interaction of electron donor and acceptor. Polyaniline acts as an electron donor in the nanocomposite [51]. Similar optical degradation behavior was reported for MNZ and other antibiotics [7,49]. These findings suggest that pH of MNZ solution is an important factor in photocatalysis under both UV and visible light radiation. Therefore most of the experiments were performed in neutral pH.

3.2.2. Effect of nanocomposite dose and weight percentage of aniline

Photocatalyst dose is one of the important factors which strongly affects degradation efficiency of contaminants [57]. The effect of TiO_2/Pani nanocomposite dose on photocatalytic degradation of MNZ was investigated in
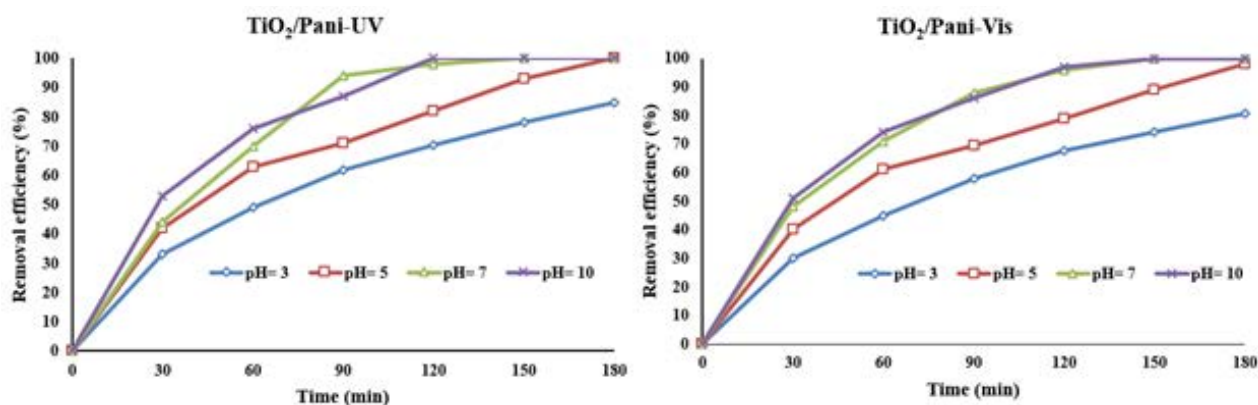

Fig. 8. Effect of primary pH on MNZ removal efficiency in TiO_2/Pani photocatalysis under UV and visible light radiation (catalyst dose 1.0 g L^{-1}, MNZ concentration 10 mg L^{-1}).
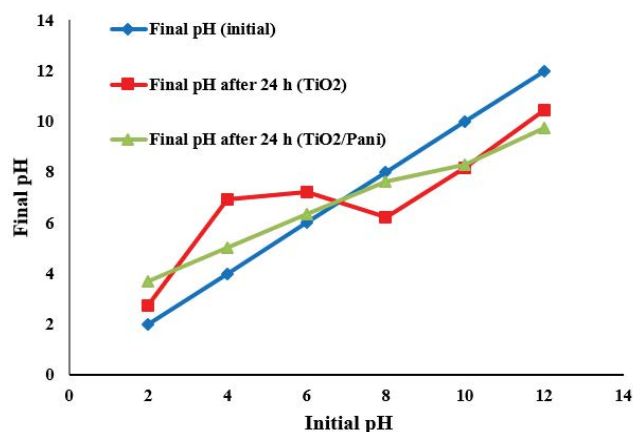
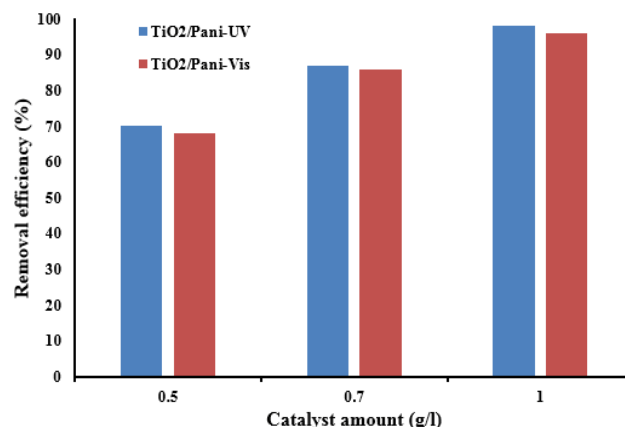Fig. 9. pH$_{zpc}$ for TiO$_2$ and TiO$_2$/Pani nanocomposite.

Fig. 10. Effect of catalyst dose on MNZ removal efficiency in TiO$_2$/Pani photocatalysis under UV and visible light radiation (MNZ concentration 10 mg L^{-1}, optimum pH 7.0, radiation time 120 min for UV and 150 min for visible light).

aqueous solution under UV and visible light radiation using 0.5–1.0 mg L^{-1} of the nanocomposite, 10 mg L^{-1} of MNZ and pH 7.0 (Fig. 10). As you see, by increasing the photocatalyst dose from 0.5 to 1.0 mg L^{-1} in 120 min under UV and visible light radiation, degradation efficiency is increased from 70% to 98% and 68% to 96%, respectively. Therefore, the degradation efficiency of MNZ is directly related to nanocomposite dose. Furthermore, useful dose of TiO$_2$/Pani nanocomposite for MNZ degradation with a primary concentration of 10 mg L^{-1} was determined 1.0 mg L^{-1}. By increasing photocatalyst dose and surface, the number of absorbed photons and MNZ molecules are also increased which consequently increases the reaction sites for production of active energy radicals, such as hydroxyl and superoxide. Increasing the photocatalyst dose higher than the optimum concentration reduces removal efficiency due to the increase of solution turbidity and light dispersion effect of suspension, which prevents sunlight transmission [49,51,58]. Effect of different weight percentages of aniline in the synthetic TiO$_2$/Pani was investigated on photocatalytic degradation of MNZ (10 g L^{-1})

under UV and visible light radiation in pH 7.0. As shown in Fig. 11, high MNZ degradation efficiency was observed in TiO$_2$/Pani nanocomposite with weight percentage of 5% after 2 h of exposure to UV and visible light. It was also found that by increasing the weight percentage of photocatalyst to 1.0, 5.0, and 10, degradation efficiencies under UV and visible light after 2 h were, respectively, 78%, ~98%, 88% and 82%, ~96%, 89%. Moreover, due to high photocatalytic activity in longer exposure times, the difference between effects of 5.0% and 10% was not obvious. This can be due to the coated Pani on the surface of TiO$_2$ in higher weight percentages which relatively prevents light transmission and contact of MNZ and photocatalyst molecules. Photocatalysis is decreased in lower weight percentages due to lower sensitization and electron production and reduction of the synergic effect between Pani and TiO$_2$. Therefore, further experiments were carried out
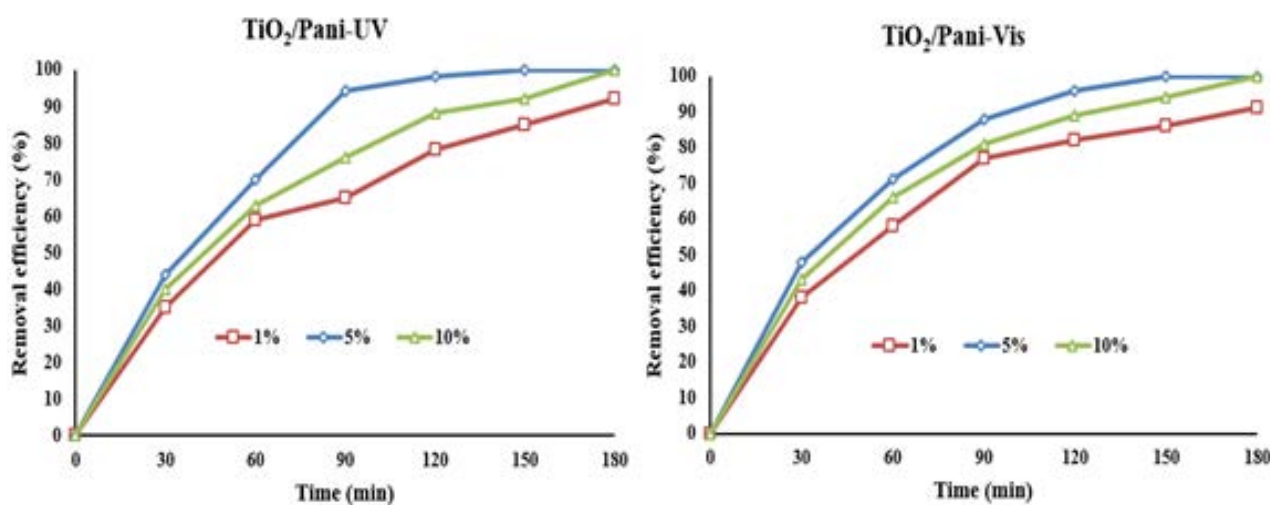

Fig. 11. Effect of different weight percentages of aniline on MNZ removal efficiency in TiO$_2$/Pani photocatalysis under UV and visible light radiation (catalyst dose 1.0 g L^{-1}, MNZ concentration 10 mg L^{-1}, optimum pH 7.0).

with TiO$_2$/Pani nanocomposite with weight percentage of 5% and similar findings were reported [41,58,59].

3.2.3. Effect of primary concentration of metronidazole

Concentration of contaminant is one of the important factors affecting photocatalysis degradation efficiency [6]. Effect of primary concentration of antibiotic on photo-catalytic degradation of MNZ was studied as a function of time under UV and visible light radiation on different concentrations of MNZ (from 10 to 40 mg L^{-1}) with a constant dose of photocatalyst (1.0 g L^{-1}; Fig. 12). As shown in the figure, maximum degradation efficiency was obtained using 10 mg L^{-1} of MNZ. This can be explained by the fact that by increasing primary concentration of antibiotic, with constant catalyst concentration and light radiation intensity, active sites for production of reactive radicals are unchanged and thus certain radicals are utilized for degradation of the increased organic molecules [21]. This effect can reduce the efficiency of MNZ degradation. In a study by Farzadkia et al. [6,49], photocatalytic degradation of MNZ was studied using ZnO and TiO$_2$ nanoparticles under radiation and it was found that the efficiency of process was reduced with increase of MNZ concentration. Similar results were reported by Debnath et al. [58], Özbay et al. [37], and Olad and Nosrati [25].

3.3. Comparison of different photocatalytic processes in metronidazole removal

For assessment and comparison of TiO$_2$/Pani oxidative photocatalysis, MNZ degradation was investigated as a function of time on different catalysts under UV and visible light radiation (Fig. 13). In a 2 h reaction time, the amount of MNZ degraded through direct photolysis, adsorption, and photocatalytic activity of TiO$_2$ and TiO$_2$/Pani was 3%, 43%, ~92%, and 98% as well as 2%, 43%, 4.9%, and ~96%, respectively, under UV and visible light, respectively (Fig. 13). In a 3 h period of UV exposure, MNZ degradation efficiency through both photocatalytic activities of TiO$_2$ and TiO$_2$/Pani was ~100%. Direct photolysis rate of MNZ with TiO$_2$/Pani
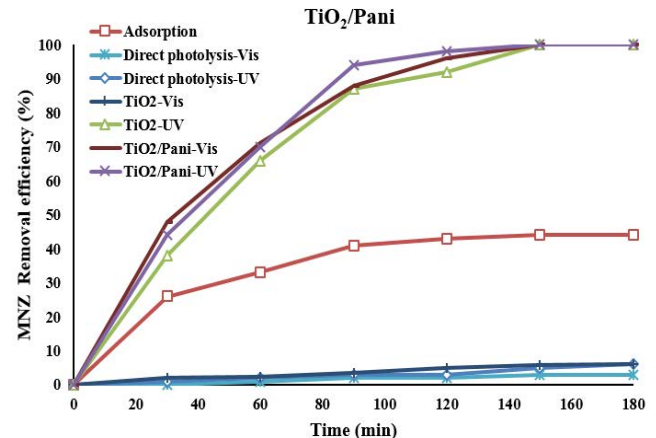
Fig. 13. Alterations of MNZ concentration in adsorption process (without light radiation), photolysis, and photocatalysis in TiO$_2$ and TiO$_2$/Pani under UV and visible light radiation (catalyst dose 1.0 g L^{-1}, MNZ concentration 10 mg L^{-1}, optimum pH 7.0).

nanocomposite was very lower comparing with adsorption and photocatalysis. Furthermore, it was revealed that MNZ degradation with TiO$_2$/Pani nanocomposite was mainly achieved by photocatalysis, not adsorption. Presence of TiO$_2$/Pani nanocomposite results in efficient photocatalytic degradation of MNZ and the degradation rate was relatively high. Photocatalytic degradation of MNZ with TiO$_2$ and TiO$_2$/Pani under UV radiation was the fastest among all of the experiments.

According to several reports, kinetics for photocatalytic degradation of organic contaminants was usually based on Langmuir–Hinshelwood mechanism (Eqs. (4) and (5)) [6,36].

$$r = \frac{k_c K_{MNZ}\left[\text{MNZ}\right]}{1 + K_{MNZ}\left[\text{MNZ}\right]_0} = k_{obs}\left[\text{MNZ}\right] \qquad (4)$$

$$\frac{1}{k_{obs}} = \frac{1}{k_c K_{MNZ}} + \frac{\left[\text{MNZ}\right]_0}{k_c} \qquad (5)$$
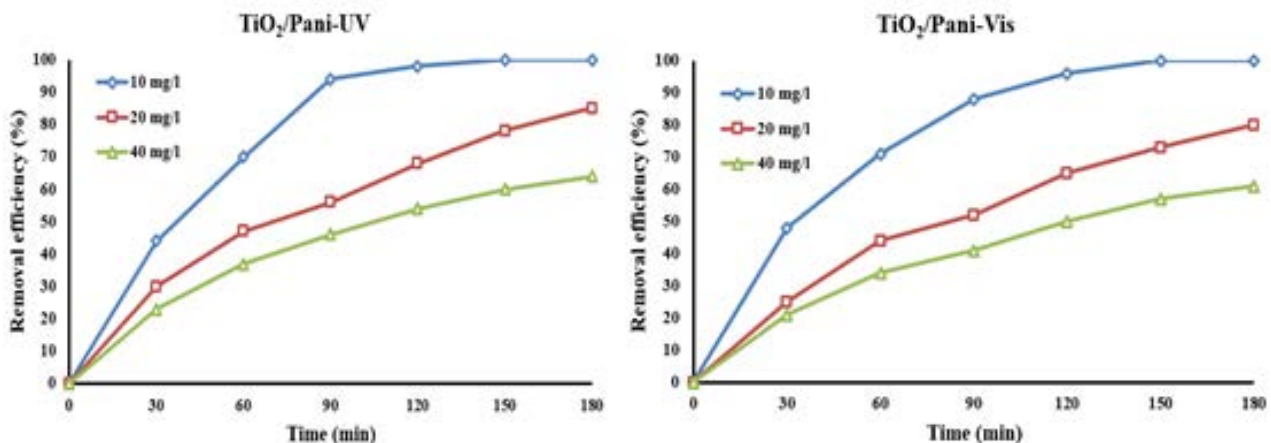
Fig. 12. Effect of primary dose of MNZ in solution on efficiency of metronidazole removal in TiO$_2$/Pani photocatalysis under UV and visible light radiation (catalyst dose 1.0 g L^{-1}, optimal pH 7.0).

where $[MNZ]_0$ represents initial concentration of MNZ (mg L^{-1}), k_c (mg L^{-1} min^{-1}) is velocity constant of the surface reaction, and K_{MNZ} (L mg^{-1}) is Langmuir adsorption coefficient [6]. The relation between initial rate constant of photocatalytic degradation (r) and initial concentration of MNZ for TiO$_2$/Pani photocatalysis was represented in Fig. 14. The k_c and K_{MNZ} values were, respectively, 0.214 and 1.98 for UV radiation and 0.185 and 1.01 for visible light.

Fig. 15 represents ln (C_0/C_t) curves against time for MNZ degradation by TiO$_2$/Pani and TiO$_2$ under UV and visible light radiation. As you see, the linear curves with correlation coefficient (R^2) near 1.0 demonstrate that TiO$_2$/Pani photocatalytic degradation kinetic in different MNZ concentrations under UV and visible light is consistent with Langmuir–Hinshelwood mechanism. Moreover, higher values of correlation coefficient show that photocatalytic degradation of MNZ by TiO$_2$/Pani follows a pseudo-first kinetic pattern. During a 2 h UV radiation period, TiO$_2$/Pani showed higher photocatalytic activity compared with visible light and TiO$_2$ samples under UV and visible light. The reaction kinetic constant for MNZ concentration of

Fig. 14. Relationship between degradation rate and initial concentration of MNZ in TiO$_2$/Pani photocatalysis under UV and visible light radiation.

10 mg L^{-1} at the TiO$_2$/Pani photocatalytic process under UV and visible light were, respectively, 0.0387 and 0.0286 min^{-1}. The rate of MNZ degradation under UV was approximately 1.35 folds over visible light (Fig. 15).

When exposed to UV, TiO$_2$/Pani nanocomposites showed relatively higher photocatalytic activity compared with TiO$_2$ under UV. The reaction kinetic constant for 10 mg L^{-1} of MNZ were 0.0387 and 0.0237 min^{-1} for TiO$_2$/Pani and TiO$_2$ under UV, respectively. Therefore, TiO$_2$/Pani photocatalysis under UV was approximately 1.63 folds over pure TiO$_2$ (Fig. 15). These results were in accordance with the studies performed by Zhang et al. [24] and Guo et al. [40].

When exposed to visible light, TiO$_2$ nanoparticles showed weak photocatalytic activity which could be related to the large gap band of TiO$_2$ (3.2 eV). Photocatalytic activity of TiO$_2$/Pani nanocomposite was much higher than TiO$_2$ when exposed to visible light and the rate constant (k) was 0.0286 min^{-1} which is approximately 95.3 folds over pure TiO$_2$ (k = 0.0003 min^{-1}) (Fig. 15). High efficiency of MNZ degradation by TiO$_2$/Pani, comparing with TiO$_2$ nanoparticles, demonstrates its higher photocatalytic activity. In general, high photocatalytic activity which was observed under both of light resources might be due to the small energy band gap of TiO$_2$/Pani nanocomposites. Because of the absorption spectrum for TiO$_2$/Pani (Fig. 6), remarkable absorption was observed in the range of 300–700 nm which indicates the ability to absorb both UV and visible light. Furthermore, polyaniline causes the improvement of several characteristics such as high visible light absorption, mobility enhancement of charge carriers, and the ability to act as electron donor in catalyst. These were consistent with several other investigations [36,59]. Hence, virtually similar activity can be observed under both UV and visible light radiation. These findings demonstrate that TiO$_2$/Pani nanocomposites are very active and can be used for purification of pharmaceutical sewage under visible light. The rate constant and photocatalysis efficiency of TiO$_2$/Pani nanocomposite on degradation of different contaminants were compared and are summarized in Table 1. Photocatalysis efficiency varied for different contaminants and results showed that it depended on experiment condition and catalyst properties such as pH, reaction time, initial
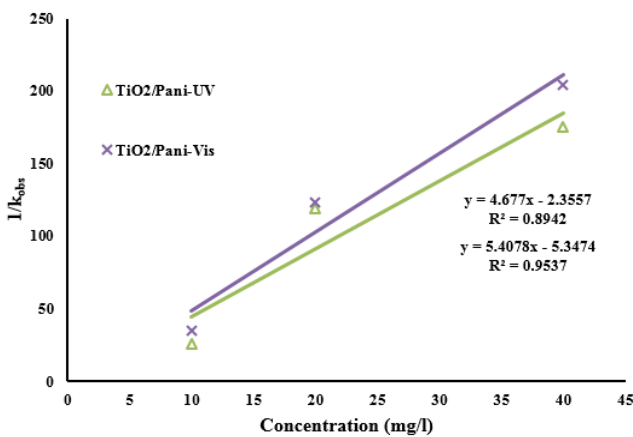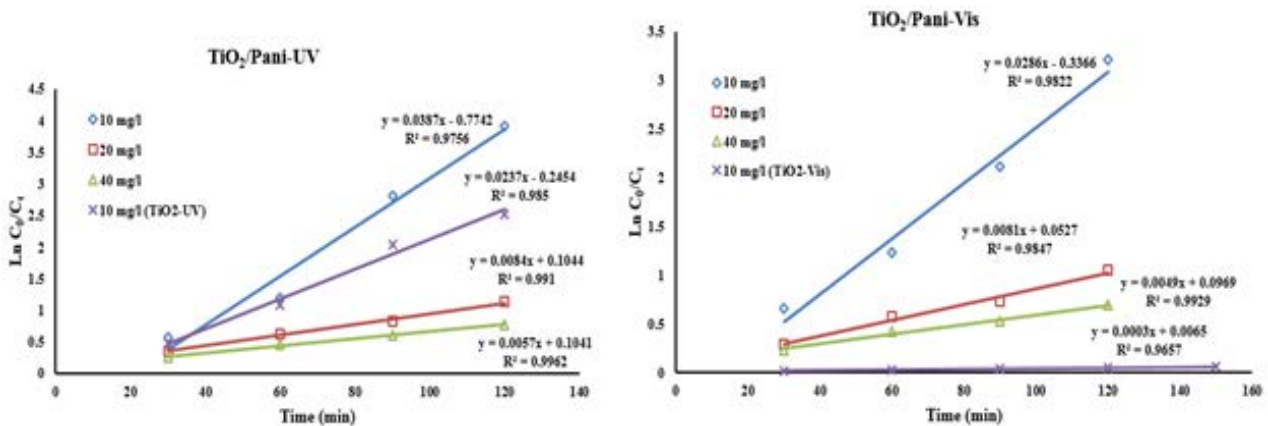

Fig. 15. Correlation of ln (C_0/C) and photocatalysis reaction time of TiO$_2$/Pani under UV and visible light radiation (catalyst dose 1.0 g L^{-1}, MNZ concentration 10 mg L^{-1}, optimum pH 7.0).

Table 1
Comparison of TiO$_2$/Pani photocatalyst application in degradation of different contaminants

Pollutant (mg L^{-1})	Light source (W)	pH	Catalyst dosage (g L^{-1})	Time (min)	Removal efficiency (%)	k_{obs} (min^{-1})	References
Reactive Blue 19(50)	Visible (–)	3.0	1.0	120	100	–	[21]
Reactive Blue 19(50)	UV (18)	3.0	1.0	120	98.4	–	[21]
Methylene Blue (10)	Visible (500 Xenon)	–	0.5	300	88	0.0071	[24]
Rhodamine B (10)	Visible (500 Xenon)	–	0.5	100	97	0.023	[24]
Methylene Blue (10)	UV (11)	–	0.5	60	99.6	0.091	[24]
Rhodamine B (10)	UV (11)	–	0.5	30	96.5	0.099	[24]
Methyl Orange (80)	UV (175)	6.0	2.5	120	95	0.036	[40]
Congo red (100)	UV (175)	6.0	2.5	120	98	0.044	[40]
Methyl Orange (80)	Natural sunlight	6.0	2.5	120	90	0.031	[40]
Congo red (100)	Natural sunlight	6.0	2.5	120	96	0.037	[40]
Ethylene diamine tetraacetic acid (20)	Visible (500 Xenon)	–	0.6	130	94	0.0197	[36]
Tartrazine (100)	UV (10)	6.8	0.05	170	99	0.029	[60]
Phenol (50)	Visible (300 Halogen)	–	1.0	600	~97	0.00314	[61]
4-Chlorophenol (10)	Visible (500 Xenon)	–	0.5	420	82.4	0.00335	[62]
Metronidazole (10)	UV (36)	7.0	1.0	120	98	0.0387	Present study
Metronidazole (10)	Visible (300 Xenon)	7.0	1.0	120	96	0.0286	Present study

concentration of contaminant, catalyst loading and size, etc. In general, the results proved that TiO$_2$/Pani photocatalyst was active under visible light and could be used for purification of different organic contaminants under visible and sun light. Moreover, one of the benefits of TiO$_2$/Pani photocatalysis is the absence of oxidant and additional chemical materials and energy when using the natural sunlight.

3.3.1. Mineralization of metronidazole and nanocomposite stability test

For monitoring the photocatalysis process in terms of intermediate compounds produced during MNZ degradation it is essential to determine total organic carbon (TOC), chemical oxygen demand (COD), and average oxidation state (AOS) during radiation [6]. Therefore, TOC, COD, and AOS values were measured under UV and visible light during radiation (Fig. 16). After 120 min of exposure, MNZ degradation efficiency under UV and visible was successively 44% and 43% for TOC as well as 100% and 99.9% for COD. TOC results demonstrated the presence of organic intermediates with difficult mineralization potential. According to COD results, degradation efficiency was increased throughout the reaction. In fact, in TiO$_2$/Pani photocatalysis system, reduction of COD was much more than TOC, which is in consistence with other studies [36,62,63]. Reduction of COD together with increase of reaction time demonstrates degradation of contaminator in photocatalysis [21]. Fig. 16 crepresents trend of changes in AOS in optimal condition under UV and visible light. As you see, the solution containing 10 mg L^{-1} MNZ is almost non-biodegradable and toxic with an AOS value of −0.97. However, TiO$_2$/Pani photocatalysis remarkably increased the AOS amounts. After oxidation, AOS values were shifted from negative to positive

under both UV and visible and reached to maximum of +4. These results confirm that MNZ was sufficiently oxidized and could be changed to biodegradable products [63].

Cyclic degradation tests were carried out for photocatalyst stability and reusability (Fig. 17). After each level of degradation, the catalyst was separated by centrifugation and used for the next cycle without any purification [59]. Hence, six successive photocatalysis experiments were performed by TiO$_2$/Pani. As presented in Fig. 17, similar photocatalytic activity was observed for the experiments under UV and visible which was in accordance with other studies [59].

3.3.2. Mechanism of photocatalysis

It is well known that TiO$_2$ alone cannot be sensitized by visible light. Schematic diagram of the possible reaction for photocatalytic degradation of MNZ using TiO$_2$/Pani is presented in Eqs. (6)–(11). Mechanism of photocatalytic oxidation of different antibiotics was discussed in several studies [7,12,13]. Photocatalytic processes for MNZ degradation under UV and visible light radiation on TiO$_2$/Pani nanocomposites are presented in Fig. 18.

Combination of TiO$_2$ with Pani results in the induction of visible light absorption (Eq. (5)). When TiO$_2$/Pani nanocomposites are exposed to visible light, TiO$_2$ acts as acceptor of the photogenerated electrons in heterojunction band of the photocatalyst, due to the fact that the conduction band of TiO$_2$ is lower than the lowest unoccupied molecular orbital (LUMO) of Pani. Pani absorbs visible light to reach the excited state. The excited electrons can then be easily injected to the conduction band of TiO$_2$ where they react with O$_2$ to produce $^\bullet$O$_2^-$ radicals (Eq. (7)). Moreover, stimulated Pani can react with OH$^-$ or H$_2$O to produce $^\bullet$OH (Eq. (8)). Both $^\bullet$O$_2^-$ and $^\bullet$OH are very reactive radicals capable
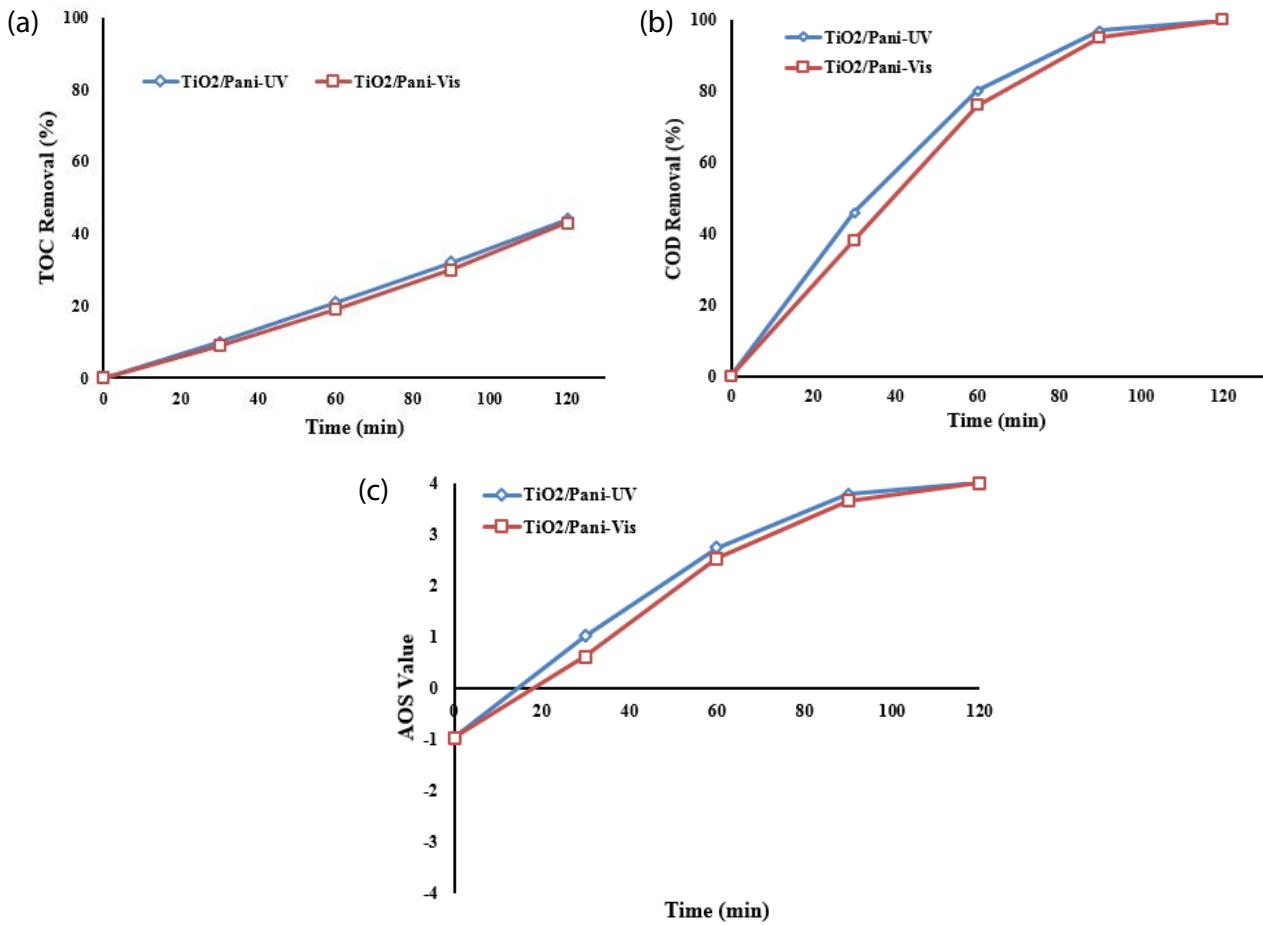
Fig. 16. Removal percentage of TOC, COD and AOS in TiO_2/Pani photocatalysis for degradation of MNZ under UV and visible light radiation (catalyst dose 1.0 g L^{-1}, MNZ concentration 10 mg L^{-1}, optimum pH 7.0).
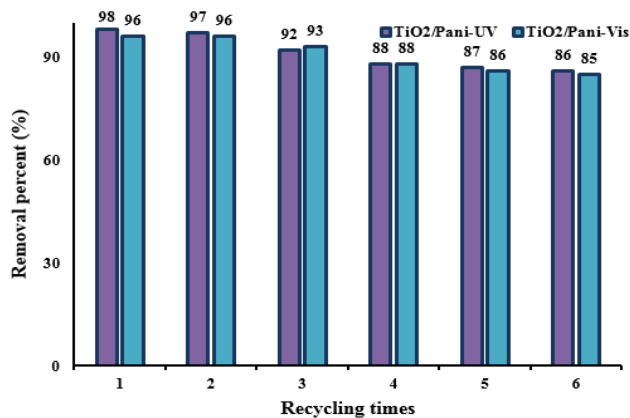

Fig. 17. Reusability test of TiO_2/Pani nanocomposite for photocatalytic degradation of MNZ in six successive experiments under UV and visible light radiation (catalyst dose 1.0 g L^{-1}, MNZ concentration 10 mg L^{-1}, optimum pH 7.0).

of oxidizing MNZ. Consequently, MNZ is degraded in TiO_2/Pani nanocomposite.

When TiO_2/Pani nanocomposites were exposed to UV, both TiO_2 and Pani absorbed photons to produce electron–
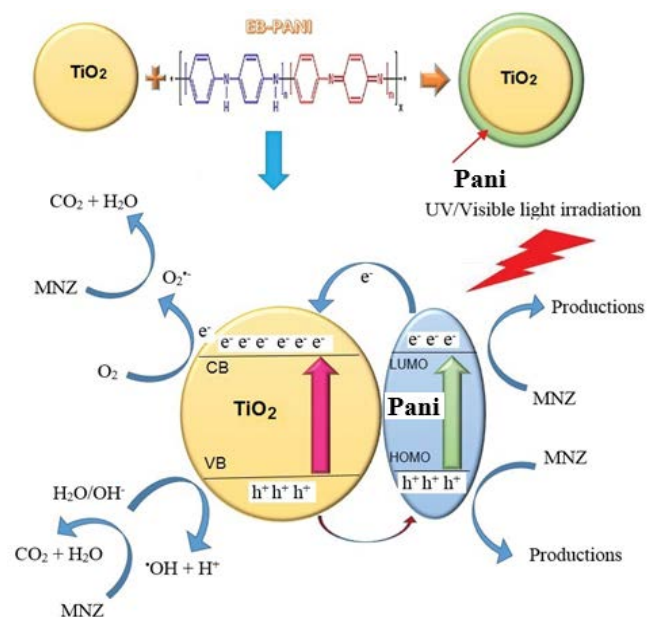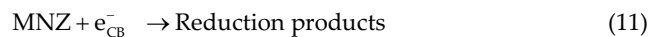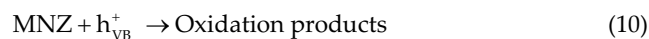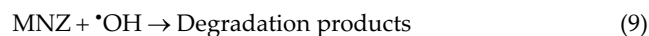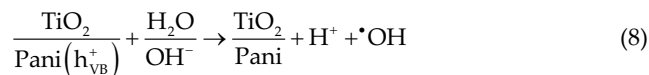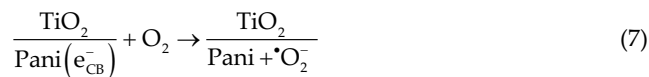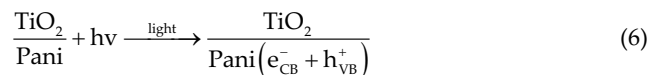

Fig. 18. Schematic diagram of photocatalyst in TiO_2/Pani nanocomposite under UV and visible light radiation.

hole pairs. Relative energy value of Pani and TiO_2 produced a synergic effect [36,51,59]. The photogenerated holes in the VB of TiO_2 could be directly transmitted to the highest occupied molecular orbital (HOMO) of Pani. Concurrently, the photogenerated electrons can be transmitted to the conduction band of TiO_2. This resulted in charge separation and stability which prevents charge recombination process [36].

The photogenerated holes (h_{VB}^+) can also oxidize organic molecules or react with OH^- or H_2O to produce $^\bullet OH$ radicals which are extremely oxidative (Eqs. (9)–(11)). Heterogeneous photocatalytic degradation of different antibiotics is summarized in the formula below [59]:

$$\frac{TiO_2}{Pani} + hv \xrightarrow{\text{light}} \frac{TiO_2}{Pani\left(e_{CB}^- + h_{VB}^+\right)} \tag{6}$$

$$\frac{TiO_2}{Pani\left(e_{CB}^-\right)} + O_2 \rightarrow \frac{TiO_2}{Pani + {}^\bullet O_2^-} \tag{7}$$

$$\frac{TiO_2}{Pani\left(h_{VB}^+\right)} + \frac{H_2O}{OH^-} \rightarrow \frac{TiO_2}{Pani} + H^+ + {}^\bullet OH \tag{8}$$

$$MNZ + {}^\bullet OH \rightarrow \text{Degradation products} \tag{9}$$

$$MNZ + h_{VB}^+ \rightarrow \text{Oxidation products} \tag{10}$$

$$MNZ + e_{CB}^- \rightarrow \text{Reduction products} \tag{11}$$

For investigating the role of active species in photocatalysis, some of scavengers were utilized for detection of the related reactive species produced by photocatalysis [36]. Ammonium oxalate (AO), benzoquinone (BQ), and tert-butanol (*t*-But) were employed as quenchers for hole (h^+), superoxide anion ($^\bullet O_2^-$), and hydroxyl radical ($^\bullet OH$), respectively.

The results showed that efficiency of MNZ photocatalysis using TiO_2/Pani nanocomposite under UV was extremely decreased when BQ, AO, and *t*-But were added to the system (Fig. 19). Based on the results, all three reactive species played same roles in MNZ degradation under UV. As presented in Fig. 19, MNZ degradation efficiency under visible light was extremely reduced when *t*-But and BQ were added to the system. According to the results, $^\bullet O_2^-$ and $^\bullet OH$ radicals were the main reactive species in photocatalytic degradation of MNZ. Similar results were reported by other investigators [59,64].

4. Conclusion

In the present study, TiO_2/Pani nanocomposite was successfully synthesized by chemical in situ polymerization of aniline. The photocatalyst was detected by FTIR, FESEM, EDX, UV–Vis DRS, and TGA methods and the results showed that polyaniline existed on TiO_2 surface and not also did not affect the structure and size of TiO_2 nanoparticles but increased their response to visible light. TiO_2/Pani nanocomposite showed high photocatalytic activity on MNZ degradation in aqueous solutions under UV and visible light such that the degradation was observed at neutral pH. Removal efficiency was reduced by increasing the dose of TiO_2/Pani and primary dose of MNZ and TiO_2/Pani had better performance (5% wt.).

Photocatalytic activity of TiO_2/Pani nanocomposite on MNZ degradation in aqueous solutions under UV and visible light was mostly assessed and compared with TiO_2. TiO_2/Pani showed higher photocatalytic activity than TiO_2. Kinetic studies, COD, TOC, AOS, nanocomposite reusability, and degradation mechanism were considered in optimal conditions.

As a mineralization index, AOS amounts were obtained in optimal condition during photocatalysis which were remarkably increased. The reduction trends in final degradation efficiency were, respectively, 9% and 8% after six successive experiments under UV and visible. Therefore, the results demonstrated that TiO_2/Pani nanocomposite was very stable and could be used several times. Based on the results, improvement of visible light absorption, the formed heterogeneous surface, rapid charge separation, reduction
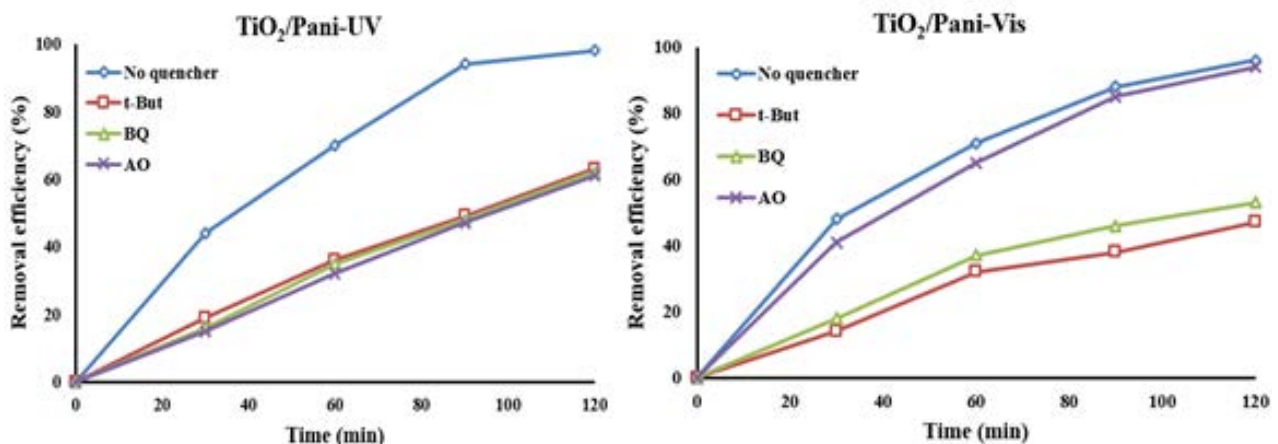

Fig. 19. Effect of different quenchers on TiO_2/Pani photocatalysis efficiency under UV and visible light radiation (catalyst dose 1.0 g L^{-1}, MNZ concentration 10 mg L^{-1}, optimum pH 7.0).

of electron–hole pair recombination, and production of $^\bullet OH$ and $^\bullet O_2^-$ radicals were all responsible for high photocatalytic activity and oxidation properties of TiO_2/Pani nanocomposite. Finally, TiO_2/Pani photocatalysis was determined as a promising method for removal of MNZ under visible light with high efficiency in a relatively short reaction time. This study provides new insights for development of reactive nanocomposites in visible light spectrum employing for photocatalytic processes.

Acknowledgments

References

[1] M.B. Ahmed, J.L. Zhou, H.H. Ngo, W. Guo, Adsorptive removal of antibiotics from water and wastewater: progress and challenges, Sci. Total Environ., 532 (2015) 112–126.

[2] F. Mohammadi, A. Esrafili, H.R. Sobhi, M. Behbahani, M. Kermani, E. Asgari, Z.R. Fasih, Evaluation of adsorption and removal of methylparaben from aqueous solutions using amino-functionalized magnetic nanoparticles as an efficient adsorbent: optimization and modeling by response surface methodology (RSM), Desal. Wat. Treat., 103 (2018) 248–260.

[3] A.S. Mohammadi, M. Sardar, M. Almasian, Equilibrium and kinetic studies on the adsorption of penicillin G by chestnut shell, Environ. Eng. Manage J., 15 (2016) 167–173.

[4] M.J. Ahmed, S.K. Theydan, Microwave assisted preparation of microporous activated carbon from *Siris* seed pods for adsorption of metronidazole antibiotic, Chem. Eng. J., 214 (2013) 310–318.

[5] D. Carrales-Alvarado, R. Ocampo-Pérez, R. Leyva-Ramos, J. Rivera-Utrilla, Removal of the antibiotic metronidazole by adsorption on various carbon materials from aqueous phase, J. Colloid Interface Sci., 436 (2014) 276–285.

[6] M. Farzadkia, E. Bazrafshan, A. Esrafili, J.-K. Yang, M. Shirzad-Siboni, Photocatalytic degradation of metronidazole with illuminated TiO_2 nanoparticles, J. Environ. Health Sci. Eng., 13 (2015) 35.

[7] V. Homem, L. Santos, Degradation and removal methods of antibiotics from aqueous matrices–a review, J. Environ. Manage., 92 (2011) 2304–2347.

[8] M.N. Chong, B. Jin, C.W. Chow, C. Saint, Recent developments in photocatalytic water treatment technology: a review, Water Res., 44 (2010) 2997–3027.

[9] S. Feizpoor, A. Habibi-Yangjeh, K. Yubuta, S. Vadivel, Fabrication of TiO_2/$CoMoO_4$/PANI nanocomposites with enhanced photocatalytic performances for removal of organic and inorganic pollutants under visible light, Mater. Chem. Phys., 224 (2019) 10–21.

[10] S. Feizpoor, A. Habibi-Yangjeh, Integration of Ag_2WO_4 and AgBr with TiO_2 to fabricate ternary nanocomposites: novel plasmonic photocatalysts with remarkable activity under visible light, Mater. Res. Bull., 99 (2018) 93–102.

[11] K. Nakata, A. Fujishima, TiO_2 photocatalysis: design and applications, J. Photochem. Photobiol., C, 13 (2012) 169–189.

[12] V. Vaiano, O. Sacco, D. Sannino, P. Ciambelli, Photocatalytic removal of spiramycin from wastewater under visible light with N-doped TiO_2 photocatalysts, Chem. Eng. J., 261 (2015) 3–8.

[13] C. Zhao, M. Pelaez, X. Duan, H. Deng, K. O'Shea, D. Fatta-Kassinos, D.D. Dionysiou, Role of pH on photolytic and photocatalytic degradation of antibiotic oxytetracycline in aqueous solution under visible/solar light: kinetics and mechanism studies, Appl. Catal., B, 134 (2013) 83–92.

[14] J. Zhu, S. Wei, L. Zhang, Y. Mao, J. Ryu, N. Haldolaarachchige, D.P. Young, Z. Guo, Electrical and dielectric properties of polyaniline–Al_2O_3 nanocomposites derived from various Al_2O_3 nanostructures, J. Mater. Chem., 21 (2011) 3952–3959.

[15] R. Konta, T. Ishii, H. Kato, A. Kudo, Photocatalytic activities of noble metal ion doped $SrTiO_3$ under visible light irradiation, J. Phys. Chem. B, 108 (2004) 8992–8995.

[16] S. Rehman, R. Ullah, A. Butt, N. Gohar, Strategies of making TiO_2 and ZnO visible light active, J. Hazard. Mater., 170 (2009) 560–569.

[17] T.P. Chou, Q. Zhang, G. Cao, Effects of dye loading conditions on the energy conversion efficiency of ZnO and TiO_2 dye-sensitized solar cells, J. Phys. Chem. C, 111 (2007) 18804–18811.

[18] R. Qiu, D. Zhang, Y. Mo, L. Song, E. Brewer, X. Huang, Y. Xiong, Photocatalytic activity of polymer-modified ZnO under visible light irradiation, J. Hazard. Mater., 156 (2008) 80–85.

[19] S. Kaur, V. Singh, Visible light induced sonophotocatalytic degradation of Reactive Red dye 198 using dye sensitized TiO_2, Ultrason. Sonochem., 14 (2007) 531–537.

[20] L. Zhang, M. Wan, Polyaniline/TiO_2 composite nanotubes, J. Phys. Chem. B, 107 (2003) 6748–6753.

[21] S. Kalikeri, N. Kamath, D.J. Gadgil, V.S. Kodialbail, Visible light-induced photocatalytic degradation of Reactive Blue-19 over highly efficient polyaniline-TiO_2 nanocomposite: a comparative study with solar and UV photocatalysis, Environ. Sci. Pollut. Res., 25 (2018) 3731–3744.

[22] M. Shekofteh-Gohari, A. Habibi-Yangjeh, M. Abitorabi, A. Rouhi, Magnetically separable nanocomposites based on ZnO and their applications in photocatalytic processes: a review, Crit. Rev. Env. Sci. Technol., 48 (2018) 1–52.

[23] Z. Han, F. Qiu, R. Eisenberg, P.L. Holland, T.D. Krauss, Robust photogeneration of H_2 in water using semiconductor nanocrystals and a nickel catalyst, Science, 338 (2012) 1321–1324.

[24] H. Zhang, R. Zong, J. Zhao, Y. Zhu, Dramatic visible photocatalytic degradation performances due to synergetic effect of TiO_2 with PANI, Environ. Sci. Technol., 42 (2008) 3803–3807.

[25] A. Olad, R. Nosrati, Use of response surface methodology for optimization of the photocatalytic degradation of ampicillin by ZnO/polyaniline nanocomposite, Res. Chem. Intermed., 41 (2015) 1351–1363.

[26] P. Kannusamy, T. Sivalingam, Chitosan–ZnO/polyaniline hybrid composites: polymerization of aniline with chitosan–ZnO for better thermal and electrical property, Polym. Degrad. Stab., 98 (2013) 988–996.

[27] M. Pirhashemi, A. Habibi-Yangjeh, S.R. Pouran, Review on the criteria anticipated for the fabrication of highly efficient ZnO-based visible-light-driven photocatalysts, J. Ind. Eng. Chem., 62 (2018) 1–25.

[28] M.A. Prathap, R. Srivastava, B. Satpati, Simultaneous detection of guanine, adenine, thymine, and cytosine at polyaniline/MnO_2 modified electrode, Electrochim. Acta, 114 (2013) 285–295.

[29] S. Radhakrishnan, K. Krishnamoorthy, C. Sekar, J. Wilson, S.J. Kim, A promising electrochemical sensing platform based on ternary composite of polyaniline-Fe_2O_3-reduced graphene oxide for sensitive hydroquinone determination, Chem. Eng. J., 266 (2015) 385–385.

[30] S. Feizpoor, A. Habibi-Yangjeh, Ternary TiO_2/Fe_3O_4/CoWO$_4$ nanocomposites: novel magnetic visible-light-driven photocatalysts with substantially enhanced activity through pn heterojunction, J. Colloid Interface Sci., 524 (2018) 325–336.

[31] S. Feizpoor, A. Habibi-Yangjeh, K. Yubuta, Integration of carbon dots and polyaniline with TiO_2 nanoparticles: substantially enhanced photocatalytic activity to removal various pollutants under visible light, J. Photochem. Photobiol., A, 367 (2018) 94–104.

[32] S. Bourdo, T. Viswanathan, Graphite/polyaniline (GP) composites: synthesis and characterization, Carbon, 43 (2005) 2983–2988.

[33] M. Mousavi, A. Habibi-Yangjeh, S.R. Pouran, Review on magnetically separable graphitic carbon nitride-based nanocomposites as promising visible-light-driven photocatalysts, J. Mater. Sci. - Mater. Electron., 29 (2018) 1719–1747.

[34] A. Olad, A. Rashidzadeh, Preparation and anticorrosive properties of PANI/Na-MMT and PANI/O-MMT nanocomposites, Prog. Org. Coat., 62 (2008) 293–298.

[35] C. Fitzgerald, M. Venkatesan, J. Lunney, L. Dorneles, J. Coey, Cobalt-doped ZnO–a room temperature dilute magnetic semiconductor, Appl. Surf. Sci., 247 (2005) 493–496.

[36] W. Li, Y. Tian, C. Zhao, Q. Zhang, W. Geng, Synthesis of magnetically separable Fe_3O_4@PANI/TiO_2 photocatalyst with fast charge migration for photodegradation of EDTA under visible-light irradiation, Chem. Eng. J., 303 (2016) 282–291.

[37] B. Özbay, N. Genç, İ. Özbay, B. Bağhaki, S. Zor, Photocatalytic activities of polyaniline-modified TiO_2 and ZnO under visible light: an experimental and modeling study, Clean Technol. Environ. Policy, 18 (2016) 2591–2601.

[38] D. Wang, Y. Wang, X. Li, Q. Luo, J. An, J. Yue, Sunlight photocatalytic activity of polypyrrole–TiO_2 nanocomposites prepared by 'in situ' method, Catal. Commun., 9 (2008) 1162–1166.

[39] D. Chowdhury, A. Paul, A. Chattopadhyay, Photocatalytic polypyrrole–TiO_2–nanoparticles composite thin film generated at the air–water interface, Langmuir, 21 (2005) 4123–4128.

[40] N. Guo, Y. Liang, S. Lan, L. Liu, J. Zhang, G. Ji, S. Gan, Microscale hierarchical three-dimensional flowerlike TiO_2/PANI composite: synthesis, characterization, and its remarkable photocatalytic activity on organic dyes under UV-light and sunlight irradiation, J. Phys. Chem. C, 118 (2014) 18343–18355.

[41] L. Gu, J. Wang, R. Qi, X. Wang, P. Xu, X. Han, A novel incorporating style of polyaniline/TiO_2 composites as effective visible photocatalysts, J. Mol. Catal. A: Chem., 357 (2012) 19–25.

[42] M.O. Ansari, F. Mohammad, Thermal stability of HCl-doped-polyaniline and TiO_2 nanoparticles-based nanocomposites, J. Appl. Polym. Sci., 124 (2012) 4433–4442.

[43] Z. Zhao, Y. Zhou, W. Wan, F. Wang, Q. Zhang, Y. Lin, Nanoporous TiO_2/polyaniline composite films with enhanced photoelectrochemical properties, Mater. Lett., 130 (2014) 150–153.

[44] WEF, APHA, Standard Methods for the Examination of Water and Wastewater, American Public Health Association (APHA), Washington, D.C., USA, 2005.

[45] J.A. Melero, F. Martínez, J.A. Botas, R. Molina, M.I. Pariente, Heterogeneous catalytic wet peroxide oxidation systems for the treatment of an industrial pharmaceutical wastewater, Water Res., 43 (2009) 4010–4018.

[46] V. Gilja, K. Novaković, J. Travas-Sejdic, Z. Hrnjak-Murgić, M.K. Roković, M. Žic, Stability and synergistic effect of polyaniline/TiO_2 photocatalysts in degradation of azo dye in wastewater, Nanomaterials, 7 (2017) 412.

[47] A. Olad, S. Behboudi, A.A. Entezami, Preparation, characterization and photocatalytic activity of TiO_2/polyaniline core-shell nanocomposite, Bull. Mater. Sci., 35 (2012) 801–809.

[48] T. Nawrot, M. Plusquin, J. Hogervorst, H.A. Roels, H. Celis, L. Thijs, J. Vangronsveld, E. Van Hecke, J.A. Staessen, Environmental exposure to cadmium and risk of cancer: a prospective population-based study, Lancet Oncol., 7 (2006) 119–126.

[49] M. Farzadkia, A. Esrafili, M.A. Baghapour, Y.D. Shahamat, N. Okhovat, Degradation of metronidazole in aqueous solution by nano-ZnO/UV photocatalytic process, Desal. Wat. Treat., 52 (2014) 4947–4952.

[50] C. Yang, M. Zhang, W. Dong, G. Cui, Z. Ren, W. Wang, Highly efficient photocatalytic degradation of methylene blue by PoPD/TiO_2 nanocomposite, PLoS one, 12 (2017) e0174104.

[51] C. Yang, W. Dong, G. Cui, Y. Zhao, X. Shi, X. Xia, B. Tang, W. Wang, Enhanced photocatalytic activity of PANI/TiO_2 due to their photosensitization-synergetic effect, Electrochim. Acta, 247 (2017) 486–495.

[52] M.O. Ansari, F. Mohammad, Thermal stability, electrical conductivity and ammonia sensing studies on *p*-toluenesulfonic acid doped polyaniline: titanium dioxide (pTSA/Pani: TiO_2) nanocomposites, Sens. Actuators B Chem., 157 (2011) 122–129.

[53] A. Talaie, J.-Y. Lee, K. Adachi, T. Taguchi, J. Romagnoli, Dynamic polymeric electrodes, dynamic computer modeling and dynamic electrochemical sensing, J. Electroanal. Chem., 468 (1999) 19–25.

[54] Z.M. Tahir, E.C. Alocilja, D.L. Grooms, Polyaniline synthesis and its biosensor application, Biosens. Bioelectron., 20 (2005) 1690–1695.

[55] R. Schindler, G. Lonnemann, J. Schaeffer, S. Shaldon, K. Koch, S. Krautzig, The effect of ultrafiltered dialysate on the cellular content of interleukin-1 receptor antagonist in patients on chronic hemodialysis, Nephron, 68 (1994) 229–233.

[56] C. Zhao, H. Deng, Y. Li, Z. Liu, Photodegradation of oxytetracycline in aqueous by 5A and 13X loaded with TiO_2 under UV irradiation, J. Hazard. Mater., 176 (2010) 884–892.

[57] R. Das, M. Bhaumik, S. Giri, A. Maity, Sonocatalytic rapid degradation of Congo red dye from aqueous solution using magnetic Fe^0/polyaniline nanofibers, Ultrason. Sonochem., 37 (2017) 600–613.

[58] S. Debnath, N. Ballav, H. Nyoni, A. Maity, K. Pillay, Optimization and mechanism elucidation of the catalytic photo-degradation of the dyes Eosin Yellow (EY) and Naphthol blue black (NBB) by a polyaniline-coated titanium dioxide nanocomposite, Appl. Catal., B, 163 (2015) 330–342.

[59] X. Chen, H. Li, H. Wu, Y. Wu, Y. Shang, J. Pan, X. Xiong, Fabrication of TiO_2@PANI nanobelts with the enhanced absorption and photocatalytic performance under visible light, Mater. Lett., 172 (2016) 52–55.

[60] M. Elsayed, M. Gobara, Enhancement removal of tartrazine dye using HCl-doped polyaniline and TiO_2-decorated PANI particles, Mater. Res. Express, 3 (2016) 085301.

[61] X. Li, D. Wang, G. Cheng, Q. Luo, J. An, Y. Wang, Preparation of polyaniline-modified TiO_2 nanoparticles and their photo-catalytic activity under visible light illumination, Appl. Catal., B, 81 (2008) 267–273.

[62] G. Liao, S. Chen, X. Quan, Y. Zhang, H. Zhao, Remarkable improvement of visible light photocatalysis with PANI modified core–shell mesoporous TiO_2 microspheres, Appl. Catal., B, 102 (2011) 126–131.

[63] X. Wang, A. Wang, J. Ma, Visible-light-driven photocatalytic removal of antibiotics by newly designed C_3N_4@$MnFe_2O_4$-graphene nanocomposites, J. Hazard. Mater., 336 (2017) 81–92.

[64] X. Chen, H. Li, H. Wu, Y. Wu, Y. Shang, J. Pan, X. Xiong, Fabrication of TiO_2@ PANI nanobelts with the enhanced absorption and photocatalytic performance under visible light, Mater. Lett., 172 (2016) 52–55.